Transverse-flux tubular motors

J. F. Eastham, M.Sc., Ph.D., C.Eng., F.I.E.E., and J. H. Alwash, B.Sc.

Indexing terms: Induction motors, Machine windings, Excitation, Magnetic circuits

ABSTRACT

The paper describes a new range of tubular induction motors. Compared with the usual forms of tubular motors, in which the magnetic flux lies largely in planes that are parallel to the direction of motion, the new machines have flux paths lying transverse to this direction. Two winding arrangements are described; the first of these uses skewed coils that completely surround the secondary conductor, the second uses a double helical system. The excitation produced by these windings is in the form of a circumferentially modulated axially travelling wave, and an appropriate multilayer analysis using cylindrical geometry is presented. Experimental and theoretical results are given that show that the transverse-flux machine can provide more thrust than the conventional machine when the core-flux density is the limiting design factor.

LIST OF SYMBOLS

E = electric-field strength, V/m
H = magnetic-field strength, A/m
f = supply frequency, Hz
J' = amplitude of line-current density J_θ, A/m
λ = wavelength of exciting wave in axial direction, m
k = wavelength factor = $2\pi/\lambda$
Z_{in} = input surface impedance, Ω
ω = $2\pi f$
s = slip
r, z, θ = subscripts for cylindrical co-ordinates
ρ = resistivity
σ = conductivity
N = total number of layers considered
P_{in} = power input per metre of axial length, W/m
F_a = axial force per metre of axial length, N/m
I_n, K_n = modified Bessel functions of general complex argument
m = subscript referring to region m
r_g = current-sheet radius, m
N_1 = effective number of turns per pole per phase at the working pole pitch
p_1 = pole pitch in the axial direction, m
$\hat{I}$ = peak of phase current, A
$\hat{H}_z\hat{E}_z$, $\hat{H}_\theta\hat{H}_\theta$ = the peak value of the respective quantities, which is a function of co-ordinate r only
n = integer
B = magnetic-flux density
μ_0 = permeability of free space
μ_r = relative permeability
μ = $\mu_0\mu_r$

Subscripts:

θ, g	z, g	θ, m	z, m	the first identifies the cylindrical co-ordinates and the second the region considered
θ, N-1	z, N-1	θ, m-1	z, m-1	
θ, 1	z, 1	z, s	θ, s	

1 INTRODUCTION

The form of a conventional tubular motor may be explained with the aid of Fig. 1.[1] Fig. 1a shows the instantaneous pole pattern of a planar linear motor. If this pattern is rolled about an axis parallel to its line of action, the pole pattern of a tubular motor is produced, as shown in Fig. 1b.

The primary-coil construction may be explained in a similar manner with the aid of Fig. 2. Fig. 2a shows one phase winding of the planar motor. To convert this into the tubular form, it is rolled into a cylindrical shape by joining AA to BB and omitting the end windings. Each conductor of the original winding forms one circular coil, as shown in Fig. 2b.

It is shown in an earlier paper[2] that transverse-flux linear motors have advantages over the more conventional type of flat machine, especially in that the flux density of a core of a given thickness is independent of the pole pitch, and these machines are specially advantageous in high-speed motors designed to run on 50 Hz supplies.

Paper 6816 P, first received 5th April and in revised form 17th August 1972

Dr. Eastham and Mr. Alwash are with the Department of Electrical Engineering, Imperial College of Science & Technology, Exhibition Road, London SW7 2BT, England

It is the object of this paper to examine some new transverse-flux machines in which the construction is tubular in that the primary coils completely surround the secondary conductor, not so much because they may be required to have large pole pitches, but because the basic change of magnetic-circuit axis enables a simpler form of laminated core to be used.

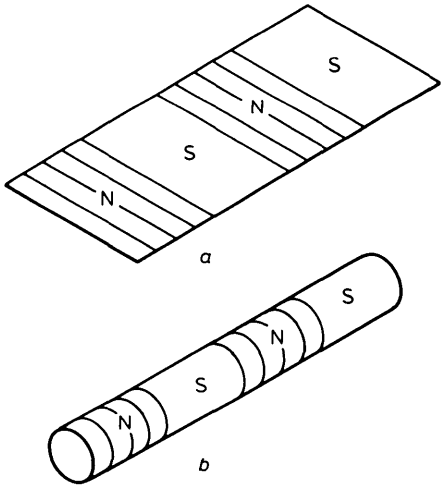

Fig. 1

Development of a conventional tubular motor

a Instantaneous pole pattern of a planar motor
b Planar motor rolled to form a tube

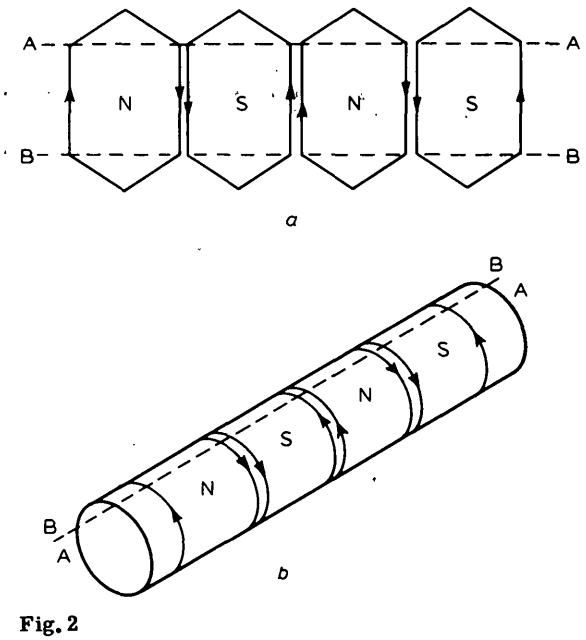

Fig. 2

Primary-coil construction for one phase of a conventional tubular motor

a Coil structure of a planar motor
b Coil structure of a tubular motor

So far, commercial tubular motors have been restricted to small sizes and low powers, so that a solid-steel core could be used without incurring severe penalties. With the expansion of the range of commercially manufactured linear motors, it is now important to investigate the design of high-powered tubular motors, and it is hoped that this paper is seen to represent a first step in the right direction.

2 NEW MACHINES

2.1 Primary-winding arrangements

2.1.1 Primary-winding arrangements using coils

The construction of the new machines may be explained by first considering a flat structure with two windings sets. This is shown in Fig. 3. As with a conventional machine, this can be rolled to form a cylinder. However, this time the end windings are not omitted, so that CC lies on DD. On the first coils of the winding sets, one coil side is shown by a heavy line. When the windings are rolled up, the points X and X' will coincide. Thus, since the points Y and Y' are also coincident,

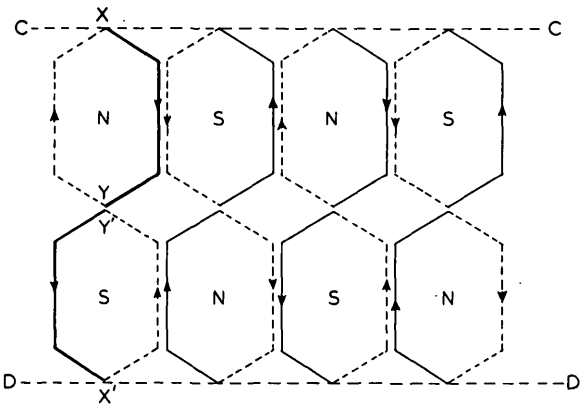

Fig. 3

Development of primary winding structure, using coils, of one phase of transverse-flux machine

the winding conductors XY and Y'X' can form a coil in the tubular form. This coil will be skewed with respect to the tube axis. Similar coils can be formed by using, in pairs, the conductors shown in plain lines. These coils form one layer of the final winding. The conductors shown by broken lines, taken together in pairs, form the second winding layer, which is skewed in the opposite direction to that of the first. Fig. 4 shows a pair of skewed coils suitable for the first coil of the winding layers.

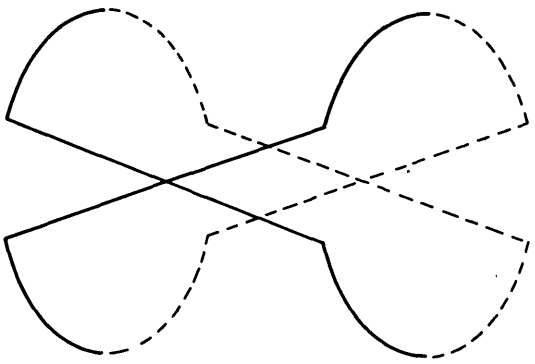

Fig. 4

Skewed coils used to construct transverse-flux-motor primary winding

The windings so far illustrated are single-phase. Polyphase windings can, of course, be constructed following the same principles. Fig. 5 shows a 1-slot-per-pole-and-phase version in which the virtual coil pitch is two-thirds of a pole pitch. It will be appreciated that any virtual double-layer winding may be formed using this coil construction. By the technique used in developing these new windings, it will be understood that they correspond with a combination of two conventional windings so arranged that the 'endturns' are coupled more closely with the secondary winding. In terms of surface windings, it will be noted that, while the system has been described in terms of the original windings having coils of conventional shape, any original coil shape is, in fact, possible.

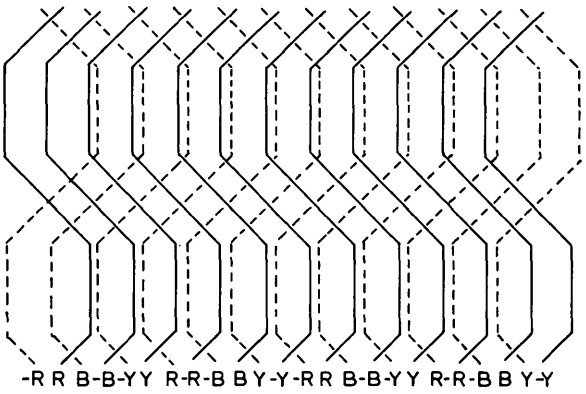

Fig. 5

3-phase version of winding using coils

2.1.2 Primary-winding arrangements using spirals

The arrangement of Fig. 3 uses conventionally shaped coils. Fig. 6 shows in broken lines a similar construction in which the coils are diamond-shaped. The plain line marked AH on this Figure represents a conductor that could replace the coil sides marked A, B; C, D; E, F; and G, H. The conductor marked IJ could similarly replace a further four coil sides. When the arrangement is rolled into tubular form, H lies on I. This means that AHIJ could be a single conductor. This conductor is helical in shape since it is at the same angle with respect to an axial line at all points in its travel. By the same

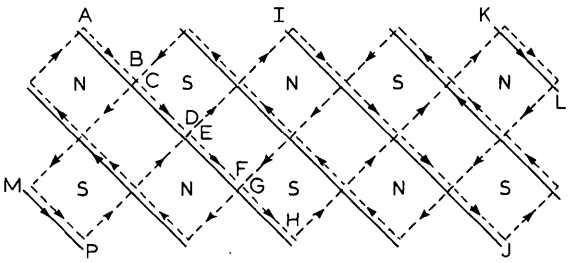

Fig. 6

Development of double helical winding

argument, the same helical conductor could be extended at each end to form MP and KL. A second helix of the same angle and pitch, but with its current oppositely directed, could replace further coil sides, as indicated in the diagram. All the coil sides that slope down from left to right have now been replaced; the pair of helixes so formed comprise the first winding layer. The coil sides that slope down from right to left may be replaced by a second pair of helical conductors. These will have the same pitch as the first pair, but will be angled in the opposite direction to form the second winding layer.

Polyphase versions of the windings may, of course, be arranged. Fig. 7 shows an unrolled 3-phase configuration; the two layers to be superimposed are shown in different diagrams, for clarity. Fig. 8 shows a sketch of the conductor shape for one layer. The winding is in the form of a 6-start thread.

The spiral windings have been described in terms of single conductors. The construction using phasebands of conductors to increase the effective number of turns is the same, but, in this situation, the conductors must be interconnected at each end of the machine; each conductor, as it emerges from, say, A, in the red phase on Fig. 7a, must be connected to a conductor at C. This leads to two possibilities. First, the conductors may be formed in spirals, and then each individual wire connected, or secondly, a long coil can be made and twisted to produce both the negative and the positive conductors of one winding layer.

The spiral winding has another feature that could be of value; if only one winding layer is used, the secondary winding will be subjected to a torque as well as a translatory force.

The windings described in Sections 2.1.1 and 2.1.2 have two poles in the circumferential direction. The system is not limited to these cases. By starting with, say, four winding sets on Fig. 3, machines with four poles in the circumferential direction can be produced.

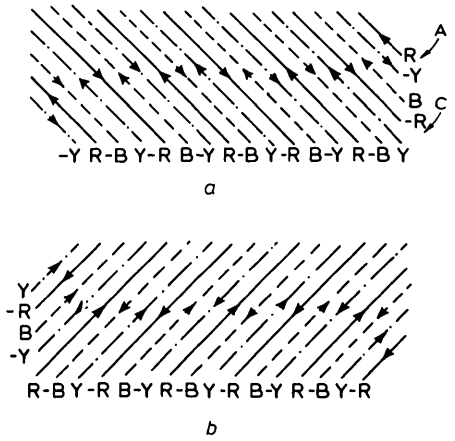

Fig. 7

3-phase helical winding arrangement

a First layer
b Second layer

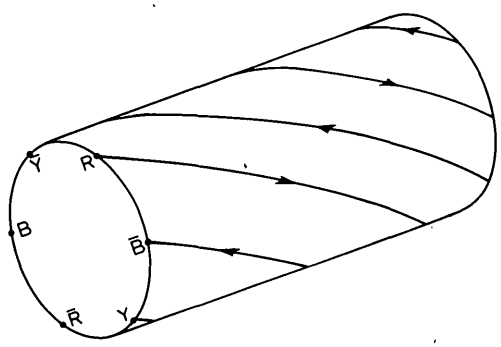

Fig. 8

One layer of a 3-phase helical winding

2.2 Magnetic circuit

Bearing in mind the original winding of Fig. 3, it will be noted that the pole flux enters the tube over one part of the periphery and leaves over a diametrically opposite area. The flux paths in the machine may now be restricted to radial and circumferential directions; i.e. the flux lies in planes that are transverse to the direction of motion, as did the flux in the planar machines described in Reference 2. Simple disc laminations may be used for the secondary. If a surface winding construction is to be used, annular laminations suffice for the primary.

The use of surface windings implies a larger magnetic gap. However, it is possible to provide a virtual 'tooth-and-slot' structure in the primary iron circuit. Fig. 9 shows a constructional drawing corresponding to a section of Fig. 5. Here, in the sloping portions, the coils are in close proximity. Thus, if the coil width remains the same, spaces are left between the straight portions. This construction, of course, corresponds to normal practice in machine windings.

The shape of lamination required to form the primary magnetic circuit is shown in Fig. 10a. A general view of the construction is shown in Fig. 10b; the windings are omitted in this Figure. It will be appreciated, however, that the sloping portions of the windings fit in the arcs labelled XX on Fig. 10a with the straight portions lying between the lamination packets. The construction of Fig. 10b could be modified by including further annular packets of laminations between those shown. These would be dimensioned as indicated at Fig. 10c and would assist in carrying the circumferential flux. This would enable the outside diameter of the machine to be reduced.

The above configurations have been developed in terms of the primary arrangement that uses coils; however, the arguments also apply to the spiral arrangement.

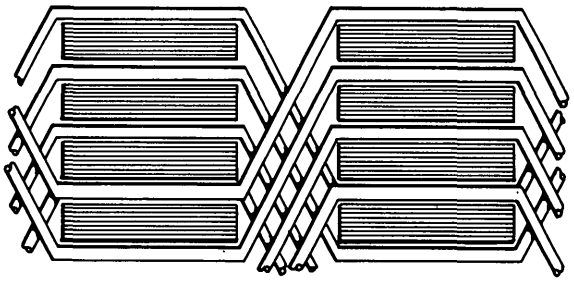

Fig. 9

Primary-lamination structure for the winding of Fig. 5

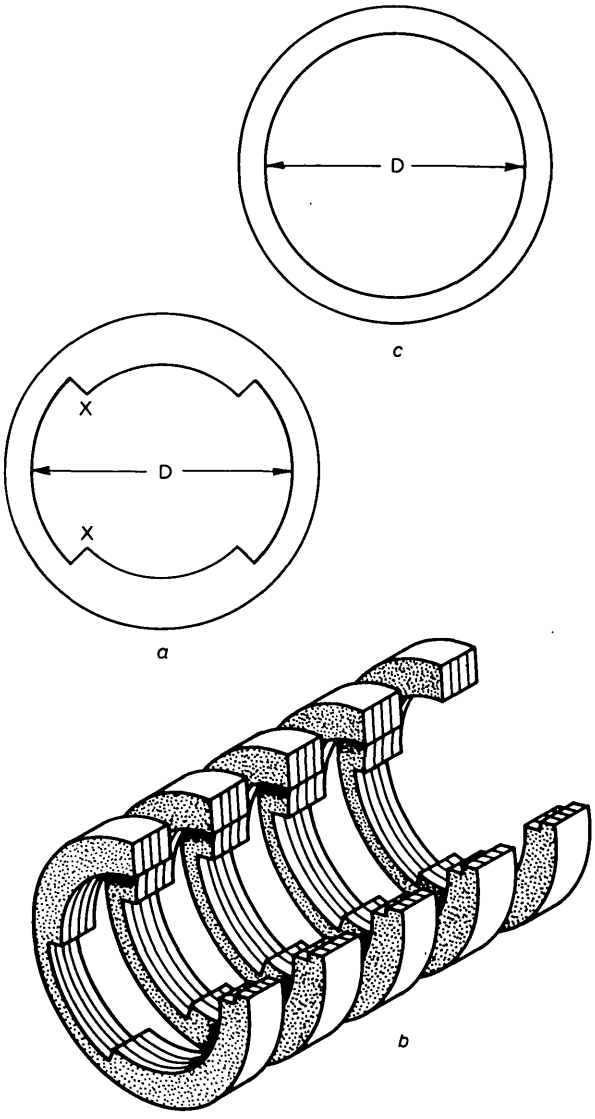

Fig. 10

Transverse-flux-motor primary-lamination structure

a Lamination shape to form the magnetic circuit of b
b Magnetic circuit
c Lamination shape if further laminations are used between the lamination packets of b

The magnetic circuits so far suggested for the new machines use laminations transverse to the direction of motion. Other lamination systems are possible; for example, Fig. 11 shows a machine in which axial lamination planes are used for the secondary magnetic circuit. Clearly, the use of this system enables the flux to take either axial or transverse secondary paths, or both. Tubular actuators in industrial use commonly have solid-steel secondary circuits. These again provide both axial and transverse flux paths. Secondary magnetic circuits providing two flux paths may be used either with machines with no primary iron circuit or with the transversely laminated circuits so far described. Equivalent primary circuits are also possible, as shown in Fig. 12. In this arrangement, slotted axial lamination packets are used to contain the primary winding. The annular punchings that surround the machine provide transverse flux paths. It is therefore possible for flux to take either transverse or axial paths.

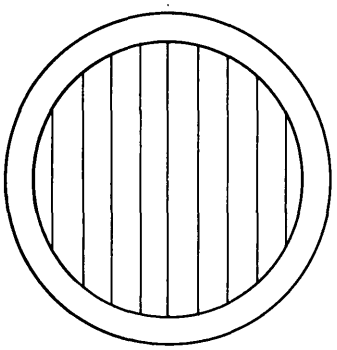

Fig. 11

Axial secondary laminations to provide both axial- and transverse-flux paths

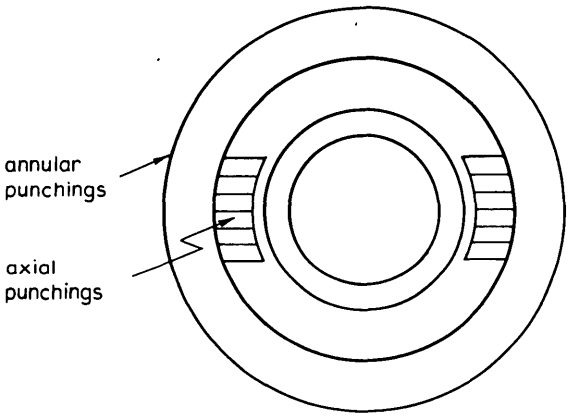

Fig. 12

Primary magnetic circuit with axial- and transverse-flux paths

3 COMPARISON WITH CONVENTIONAL MACHINES

In conventional tubular motors, the electric circuits are perfect in that no axial currents exist. That is to say, the secondary currents have circular paths only, and no endturns are required in the primary winding. However, the magnetic circuit becomes more difficult. At any section of the tube, the flux crosses the rotor conductor radially, and its direction is the same at all points on the periphery. Thus the flux from one pole of the machine must pass axially to the next pole, and the area of the rotor magnetic circuit limits the pole flux. This limitation is severe when the pole pitch is long compared with the radius. The core-flux limitation implies that the airgap flux density must be reduced as the pole pitch increases.

In the new machines, the flux has no axial component in the secondary core, and the airgap density is therefore independent of the pole pitch. The flux passes transversely through the secondary winding, and no constriction is imposed on the flux path. The magnetic circuit is therefore improved. However, the electric circuits are inferior in the new machines. First, the windings have virtual endturns, i.e. the primary conductors have axial components. Secondly, the rotor currents are constrained to paths of the form of those shown in Fig. 13. Therefore the apparent resistivity of the secondary winding viewed from the primary winding will be increased compared with that which would be obtained in the conventional case, owing to the extra path lengths involved.

Thus, as far as the ratio of the forces produced at constant core flux is concerned, as the pole pitch increases, there is a tradeoff between a reduced gap-density on one hand and an increased effective rotor resistance on the other. However, it was felt that the new machines should be better over a range of parameters, and it was therefore considered to be worthwhile to test the machines both practically and analytically. As a result, as may be seen from the following Sections, substantial increases in force can be produced.

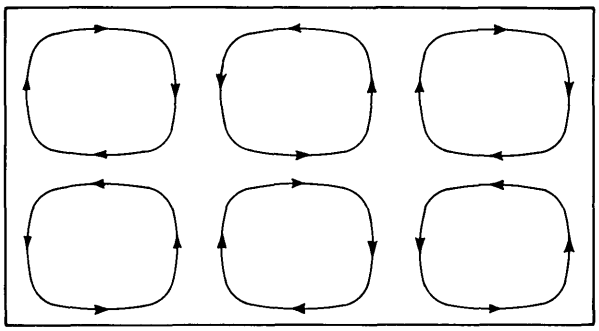

Fig. 13

Secondary-current patterns in transverse-flux tubular motors

4 THEORETICAL ANALYSIS

4.1 Primary-current density

The primary winding considered consists of two superimposed helical distributions, corresponding to the arrangement shown in Fig. 7. It is assumed that the windings produce perfect sinusoidal travelling waves.

The current density then consists of two components:

$$J_1 = \mathrm{Re}\left\{\frac{N_1\hat{I}}{2L}\exp(j\phi)\exp j(\omega t - kz + n\theta)\right\}$$

$$J_2 = \mathrm{Re}\left\{\frac{N_1\hat{I}}{2L}\exp j(\pi - \phi)\exp j(\omega t - kz - n\theta)\right\}$$

where ϕ is the angle of the winding with respect to a line parallel to the motor axis, and is given by

$$\phi = \tan^{-1}\left(\frac{kr_g}{n}\right)$$

and $L = (p_1 \sin\phi)/3$

The resultant current density can be represented by two components

$$J_z = \mathrm{Re}\ \{jJ' \cos\phi \sin(n\theta)\exp j(\omega t - kz)\}$$

$$J_\theta = \mathrm{Re}\ \{J' \sin\phi \cos(n\theta)\exp j(\omega t - kz)\} \quad (1)$$

where

$$J' = N_1\hat{I}/L \quad (2)$$

4.2 Mathematical model

A general multiregion problem is analysed. The model is taken to be a set of infinitely long concentric cylinders, with a radially infinitesimally thin and axially infinite current-sheet excitation at radius r_g.

To simplify the problem, it is assumed that the resitivity in the radial direction is infinite. In particular, this can be taken to imply that any conducting region is perfectly laminated, by being constructed from infinitely thin insulated concentric cylinders. Displacement currents are assumed to be negligible, and magnetic saturation is neglected.

Maxwell's equations for any region in the model are

$$\text{curl } H = J \tag{3}$$

$$\text{curl } E = -\frac{\partial B}{\partial t} \tag{4}$$

$$\text{div } B = 0 \tag{5}$$

$$\text{div } J = 0 \tag{6}$$

$$\text{div } E = 0 \tag{7}$$

$$J = \sigma E \tag{8}$$

$$B = \mu H \tag{9}$$

and, from the initial assumptions, we have $J_r = 0$ (10)

The boundary conditions are

(a) The radial flux density is continuous across a boundary.
(b) The axial component of magnetic field strength is continuous across a boundary, but allowance must be made for the current sheet, in the manner shown in Section 4.4.

4.3 Field equations of a general region

As a first step in the analysis, the field components of a general region are derived.

Assuming that all the fields vary as $\exp\{j(\omega t - kz)\}$, and omitting this factor for shortness, from all the field expressions that follow, we have, from eqns. 1 and 8,

$$E_\theta = \hat{E}_\theta \cos(n\theta) \tag{11}$$

Using eqns. 6, 8, 11, 4, 9 and 7, and assuming $\sigma_z = \sigma_\theta = \sigma$ and $J_r = 0 (\sigma_r = 0)$, it can be shown that, for $n \neq 0$, we have

$$\hat{E}_z = \frac{jn}{kr}\hat{E}_\theta \tag{12}$$

$$E_z = \{AI_n(\alpha r) + DK_n(\alpha r)\} \sin(n\theta) \tag{13}$$

where

$$\alpha^2 = k^2 + js\omega\mu\sigma \tag{14}$$

I_n and K_n are modified Bessel functions of order n and of general complex argument.[3] A and D are arbitrary constants to be determined from the boundary conditions.

Using eqns. 11-13, for $n \neq 0$,

$$E_\theta = \frac{-jrk}{n}\{AI_n(\alpha r) + DK_n(\alpha r)\}\cos(n\theta) \tag{15}$$

Using eqns. 4 and 11-13, it can be shown that

$$H_r = \frac{-(n^2 + k^2r^2)}{\omega\mu r^2 k} E_\theta \tag{16}$$

Then, using eqns. 1, 3, 10, 11 and 16, we have

$$\hat{H}_\theta = \frac{-jn}{rk}\hat{H}_z \tag{17}$$

$$H_\theta = \hat{H}_\theta \sin(n\theta) \tag{18}$$

$$H_z = \hat{H}_z \cos(n\theta) \tag{19}$$

Using eqns. 5 and 15-19, and assuming that $\mu_z = \mu_r = \mu_\theta = \mu$, we have

$$H_z = \frac{kr}{n\omega\mu}\left[\left(\frac{2rk^2}{n^2 + r^2k^2} - \frac{n}{r}\right)\{AI_n(\alpha r) + DK_n(\alpha r)\} + \alpha\{AI_{n-1}(\alpha r) - DK_{n-1}(\alpha r)\}\right]\cos(n\theta) \tag{20}$$

4.4 Field calculations at the region boundaries

Fig. 14a shows a general region m, where $E_{\theta,m}$ and $H_{z,m}$ are the field components at the upper boundary of the region, and $E_{\theta,m-1}$ and $H_{z,m-1}$ are the equivalent values at the lower boundary.

From eqns. 15 and 20,

$$E_{\theta,m} = \frac{-jr_m k}{n}\{AI_n(\alpha_m r_m) + DK_n(\alpha_m r_m)\}\cos(n\theta) \tag{21}$$

$$H_{z,m} = \frac{kr_m}{n\omega\mu_m}\left[\left(\frac{2r_m k^2}{n^2 + r_m^2 k^2} - \frac{n}{r_m}\right)\{AI_n(\alpha_m r_m) + DK_n(\alpha_m r_m)\} + \alpha_m\{AI_{n-1}(\alpha_m r_m) - DK_{n-1}(\alpha_m r_m)\}\right]\cos(n\theta) \tag{22}$$

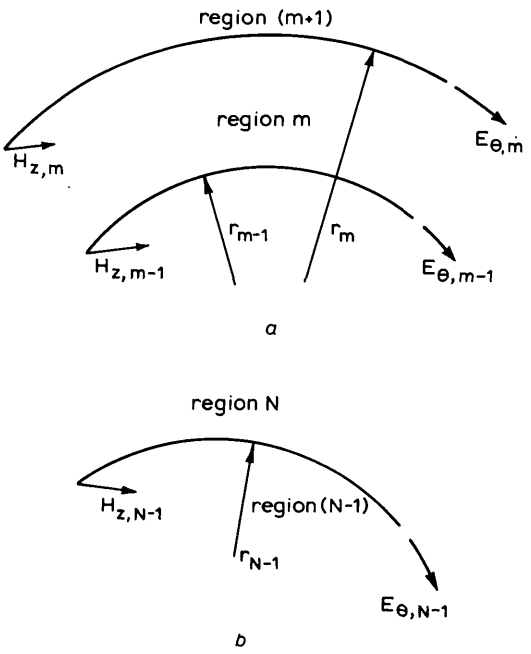

Fig. 14

Mathematical model

Equivalent expressions for $E_{\theta,m-1}$ and $H_{z,m-1}$ can be formed by replacing r_m in the above equations by $r_{(m-1)}$.

Now, for the regions where $m \neq 1$ or N,

$$\begin{bmatrix} E_{\theta,m} \\ H_{z,m} \end{bmatrix} = \begin{bmatrix} T_m \end{bmatrix} \begin{bmatrix} E_{\theta,m-1} \\ H_{z,m-1} \end{bmatrix} \tag{23}$$

where $[T_m]$ is the transfer matrix[4,5] for region m, and is given by

$$\begin{bmatrix} T_m \end{bmatrix} = \begin{bmatrix} a_m & b_m \\ c_m & d_m \end{bmatrix} \tag{24}$$

Expressions for a_m, b_m, c_m and d_m are derived in Appendix 9.

Hence, given the E_θ and H_z at the lower boundary of a region, the E_θ and H_z at the upper boundary can be found using this transfer matrix. At the boundaries where no excitation-current sheet exists, we have continuity of H_z and E_θ; thus, for example, if two regions are considered with no current sheet at the common boundary, knowing H_z and E_θ at the beginning of the first region, H_z and E_θ at the end of the second region may be calculated by successive use of the two transfer matrices. Considering the current sheet to be at radius r_g,

$$H'_{z,m} = H_{z,m} \qquad m \neq g \tag{25}$$

and

$$H'_{z,m} = H_{z,m} - J_\theta \quad m = g \tag{26}$$

where $H_{z,m}$ is the axial magnetic field strength immediately below a boundary and $H'_{z,m}$ is the axial magnetic field strength immediately above a boundary.

Bearing in mind the boundary conditions, it is apparent that, for the model considered, we can write

$$\begin{bmatrix} E_{\theta,N-1} \\ H_{z,N-1} \end{bmatrix} = \begin{bmatrix} T_{N-1} \end{bmatrix} \begin{bmatrix} T_{N-2} \end{bmatrix} \cdots \begin{bmatrix} T_{g+1} \end{bmatrix} \begin{bmatrix} E_{\theta,g} \\ H_{z,g} - J_\theta \end{bmatrix} \quad (27)$$

and

$$\begin{bmatrix} E_{\theta,g} \\ H_{z,g} \end{bmatrix} = \begin{bmatrix} T_g \end{bmatrix} \begin{bmatrix} T_{g-1} \end{bmatrix} \cdots \begin{bmatrix} T_2 \end{bmatrix} \begin{bmatrix} E_{\theta,1} \\ H_{z,1} \end{bmatrix} \quad (28)$$

If region N is now considered (Fig. 14b), then, as $r \to \infty$, $I_n(\alpha r) \to \infty$. Therefore, from eqns. 21 and 22,

$$A = 0$$

$$E_{\theta,N-1} = \frac{-jr_{N-1}k}{n} DK_n(\alpha_N \sigma | r_{N-1}) \cos(n\theta) \quad (29)$$

and

$$H_{z,N-1} = \frac{kr_{N-1}}{n\omega\mu_N} \left\{ \left(\frac{2r_{N-1}k^2}{n^2 + r_{N-1}^2 k^2} - \frac{n}{r_{N-1}} \right) DK_n(\alpha_N r_{N-1}) - \alpha_N D K_{n-1}(\alpha_N r_{N-1}) \right\} \cos(n\theta) \quad (30)$$

Considering region 1, we have, as $r \to 0$, $K_n(\alpha r) \to \infty$. Therefore, from eqns. 21 and 22,

$$D = 0$$

$$E_{\theta,1} = \frac{-jr_1 k}{n} A I_n(\alpha_1 r_1) \cos(n\theta) \quad (31)$$

and

$$H_{z,1} = \frac{kr_1}{n\omega\mu_1} \left\{ \left(\frac{2r_1 k^2}{n^2 + r_1^2 k^2} - \frac{n}{r_1} \right) AI_n(\alpha_1 r_1) + \alpha_1 AI_{n-1}(\alpha_1 r_1) \right\} \cos(n\theta) \quad (32)$$

The field components at the boundaries of regions 1 and N still contain arbitrary constants. The ratios however of E_θ to H_z at these boundaries contain no arbitrary constants, and it is only these ratios that are needed for a complete solution. The following Section shows how this may be accomplished. The ratios of E_θ to H_z have been termed the surface impedance.[6-8]

4.5 Surface-impedance calculations

The surface impedance looking outwards at a boundary of radius r_s is defined as

$$Z_{s+1} = \frac{E_{\theta,s}}{H'_{z,s}} \quad (33)$$

and the surface impedance looking inwards is

$$Z_s = -\frac{E_{\theta,s}}{H_{z,s}} \quad (34)$$

Using the method outlined in Reference 8 with the values for $E_{\theta,N-1}$, $H_{z,N-1}$, $E_{\theta,1}$, $H_{z,1}$, a_m, b_m, c_m and d_m as derived in the previous Section, we obtain

$$Z_{in} = \frac{Z_g Z_{g+1}}{Z_g + Z_{g+1}} \quad (35)$$

where Z_{in} is the input surface impedance at the current sheet and Z_{g+1} and Z_g are the surface impedances 'looking' outwards and inwards at the current sheet. Substituting for Z_g and Z_{g+1}, using eqns. 34 and 33, respectively, and rearranging,

$$Z_{in} = \frac{-E_{\theta,g}}{H_{z,g} - H'_{z,g}} \quad (36)$$

Using eqn. 26,

$$H'_{z,g} = H_{z,g} - J_\theta$$

Substituting this in eqn. 36,

$$Z_{in} = \frac{-E_{\theta,g}}{J_\theta} \quad (37)$$

Thus, the input impedance at the current sheet has been determined. This means that all the field components can be found by making use of this and eqns. 34, 27 and 28.

4.6 Power calculations

The time-average power flowing through a boundary is given by the equation

$$P = \mathrm{Re}\left[\frac{1}{2\pi} \int_0^\pi \{ \hat{E}_\theta \hat{H}_z^* \cos^2(n\theta) - \hat{E}_z \hat{H}_\theta^* \sin^2(n\theta) \} d\theta \right] \text{ watts per square metre} \quad (38)$$

Then, using this, and eqns. 12, 17, 26 and 37, it can be shown that the total input power is

$$P_{in} = 0{\cdot}5\pi r_g \left(1 + \frac{n^2}{k^2 r_g^2} \right) |J'|^2 \mathrm{Re}(Z_{in}) \text{ watts per metre} \quad (39)$$

The axial force, F_a is given by

$$F_a = \frac{P_{in}}{\lambda f} \text{ newtons per unit axial length} \quad (40)$$

4.7 Computation

The method outlined above can be readily programmed for digital-computer use, and has been used to calculate the axial force and the core-flux density for the experimental model.

In this case, n is taken to be 1, which means that only the fundamental component in the θ direction is considered. However, the method is, of course, general; any number of harmonics in the θ direction can be considered in turn (by changing n to the appropriate harmonic number with the exception of n = 0) to calculate the harmonic power. Since linear magnetic conditions are assumed, the total power input can be taken to be the sum of the power harmonic components, and the total axial force is then given by,

$$F_a = \frac{\Sigma_n P_{in}}{\lambda f} \text{ newtons per metre} \quad (41)$$

4.8 Calculation of the core-flux density

The rotor core can be represented by, say, region 1 of the model. If it is assumed that this region is made of infinitely laminated iron, the contribution of $H_{z,1}$ and $H_{\theta,1}$ to the core-flux density can be neglected. This leaves only the radial component $B_{r,1}$ to be considered. This component is cosinusoidally distributed in the circumferential direction, and it will be appreciated that, since $H_{z,1}$ and $H_{\theta,1}$ are negligible, the whole of the flux from one transverse pole passes across a diameter of the core section. Thus, since the average flux density is given by $2/\pi \hat{B}_{r,1}$, the flux per metre crossing the diameter is $2/\pi \hat{B}_{r,1} \pi r_1 = 2r_1 \bar{B}_{r,1}$, so that the core-flux density, assuming that the flux is evenly distributed across the diameter, is given by $\hat{B}_c = 2r_1 \hat{B}_{r,1}/2r_1 = \hat{B}_{r,1}$.

4.9 Comparison with existing theoretical approaches for planar model

If a model is chosen so that the thickness of the layers is very small compared with the radii, it may be analysed as a planar model.

The results for such a model were obtained with the layer thicknesses of the order of 10^{-3} of the radii, first from the analysis mentioned above (Section 4.1-4.7), and secondly from a planar theory using the Preston and Reece[9] model for one harmonic, and employing for this the surface-impedance method suggested in Reference 10. The results obtained by the two methods were found to be numerically within 1% for the particular case calculated.

A conventional simple analysis, which assumed that the flux density did not vary across the machine gap, was also attempted. This again gave results consistent with the main analysis for the model considered above.

4.10 Theoretical analysis for conventional tubular motor

The power input, force and flux components have been derived using the analysis given in Reference 8.

The core-flux density is then calculated as follows. The excitation, in this case, is constant in the circumferential direction; the flux has the same direction instantaneously at all points on a circumferential line. Thus the flux from one pole must pass axially to the adjacent poles. If the tubular motor had no ends, conventional-machine conditions would apply; i.e. one-half of the flux from a particular pole would pass axially down the core to the preceding pole while the second half would pass axially to the following pole. Nix and Laithwaite[1] showed that, provided that a model having planar geometry could be assumed, the actual core densities, when end effects are accounted for, have values that are greater than the conventional value (of the order of 1·1-1·3). They also showed that the force calculated would be less than the conventional force by a factor of between 0·85 and 0·95. To produce an optimistic view of the conventional machine for comparison purposes, and in the absence of a cylindrical-geometry analysis that accounts for end effects, it was decided to treat the core flux and force on the conventional bases. Thus, if region 1 of the model is infinitely laminated iron, the core density may be calculated from the radial flux-density component using the equation

$$\hat{B}_c = \frac{2p_1}{\pi r_1}\hat{B}_{r,1} \qquad (42)$$

5 EXPERIMENTAL MACHINES

To compare the performance of the new machines with conventional tubular machines, and to verify the analysis described in the previous section, two models were made. The first of these used the coil form of construction explained in Section 2.1.1. The second was a tubular motor equivalent to the first using circular coils.

5.1 Model of the new machine

This model used a surface primary winding that was formed on a tube made from an insulating material and having a diameter $d_a = 70$ mm. The skewed coils forming the winding were made to simulate an original winding having diamond-shaped coils. The coil sides were skewed at 45° with respect to the motor axis. Fig. 15 shows a photograph of one of the coils. Twelve of these were used to form each winding layer. The surface axial length of each coil was arranged so that three coils extended over a distance of $\pi d_a/2$. The winding may be connected for either two or four poles by using either two coils or one coil per pole and phase. When the machine is connected for four poles, it also simulates a helical winding. Connection as a 2-pole machine results in a virtual chording factor of 0·707, since the winding is simulating an original structure in which the coil pitch is one-half of the pole pitch. No primary iron circuit was provided. The secondary member consisted of disc-shaped laminations contained inside a copper tube. The outside and inside diameters of this were 63·2 mm and 57·3 mm, respectively.

The analysis assumes that there is an infinitely thin current-sheet excitation. This cannot, of course, be achieved in practice. The thickness of the windings of the model is appreciable and not completely uniform. Thus the average diameter of the excitation is used in the calculations.

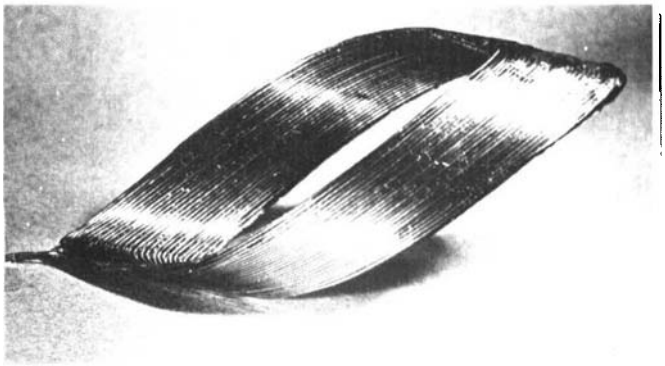

Fig. 15

One coil used in the transverse-flux experimental motor

5.2 Conventional tubular motor

This machine was constructed so that it was equivalent to the new-machine model. That is, the axial coil length and the number of the circular coils were identical. The rotor dimensions were the same, but, in this case, the rotor core was axially laminated, as shown in Fig. 11.

5.3 Experimental results

5.3.1 Flux measurements on the new machine

To verify that the excitation produced by the winding was as calculated in Section 4.1, the windings were excited, and the three flux components B_r, B_θ and B_z were measured in the absence of the secondary winding. These values were found to vary by only a small percentage (approximately 5%) along most of the tube length. The average values measured were found to be within 5% of the predicted value.

Measurements were then taken with the rotor present. It was anticipated that the axial component of core flux would be negligible; i.e. the pole flux was thought to pass transversely across the core. The analysis confirmed this prediction. To verify the point practically, a coil of the shape shown in Fig. 16 was inserted between the rotor-disc laminations. This coil should measure any flux of the form shown in the Figure. Measurements made using this coil confirmed that the axial flux was negligible along the tube length. Thus, to find the core-flux density, coils on the surface of the rotor core of the form also shown in Fig. 16 may be used. As may be seen from the Figure, five coils covering half the stator length were provided. With the field travelling in a first direction, four sets of readings were taken from the coils, the rotor being displaced by one-quarter of the search-coil pitch between successive sets. This, of course, gives readings

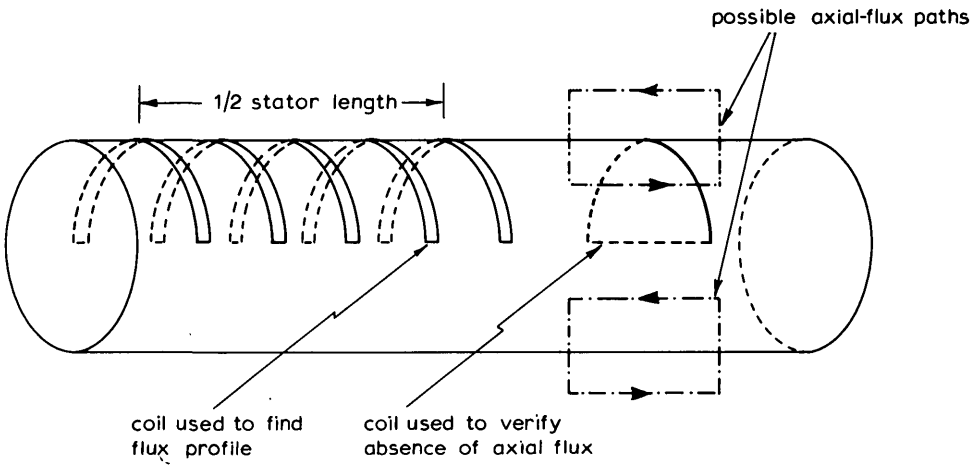

Fig. 16

Search-coil arrangements

that may be interleaved to provide a detailed flux profile over half the machine length. The process was then repeated with the field travel reversed. Fig. 17 shows the results obtained from this procedure for a 2-pole connection at 70 Hz. It will be observed that the flux is affected by the phasebands of the excitation. The broken line shown on the Figure is a suggested average value of the core flux, neglecting the values at the ends of the machine. The solid line shows the predicted result from the analysis. This process was repeated for various frequencies for both the 2- and 4-pole connections. Figs. 18 and 19 show the measured and predicted values for the 2- and 4-pole connections, respectively. It will be observed that reasonable agreement is obtained.

5.3.2 Flux measurements on the conventional machine

Five circular coils round the rotor core were provided in the same relative positions as those for the new machine, and sets of results were taken in the same manner. Fig. 17 shows a sample flux profile for one case. Again the broken line represents a suggested average flux while the solid line shows the predicted value. The process was repeated for a set of frequencies for both the 2- and the 4-pole connections. Fig. 20 shows the calculated and measured values for the 2-pole connection plotted against frequency. Again the agreement is found to be reasonable.

5.3.3 Area-correction factor for the new machine

It will be appreciated that the ends of the windings produce sections that are not complete. This may be appreciated with the aid of Fig. 21, which shows a developed view of the windings.

To assess the effect of the ends, an experiment was performed in which the excitation length was successively shortened. The pole pitch used corresponded to the 4-pole condition. Fig. 22 shows the standstill force produced at 50 Hz plotted against the number of coils omitted from each layer at one end of the winding. The theoretical force, assuming that the length of excitation present was $2\pi d_a$ in the complete winding situation, is also plotted on the Figure. It will be observed that the measured force is deficient by an amount that could be considered to be constant. This is to be

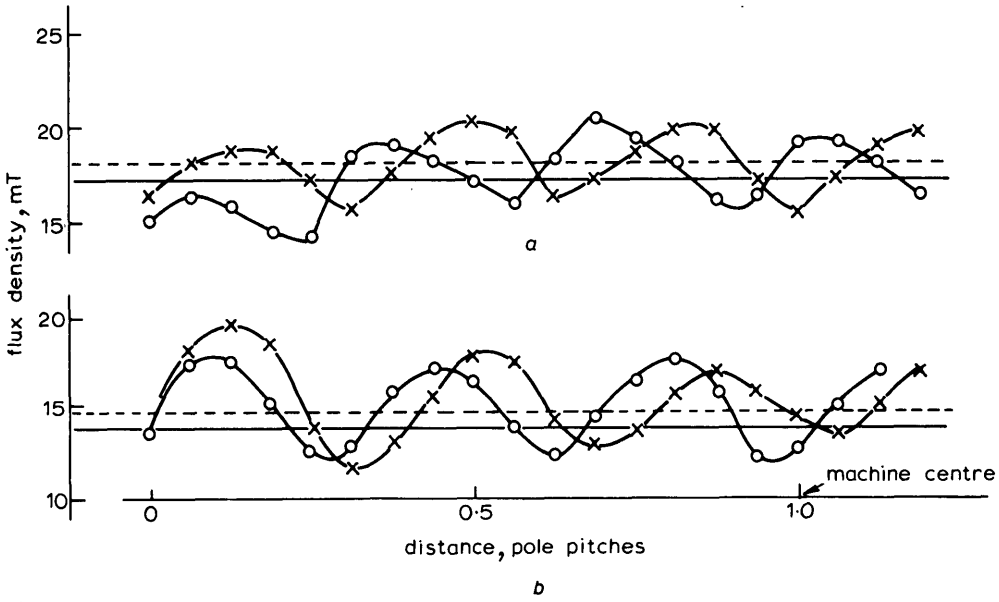

Fig. 17

Flux profiles at 70 Hz with 2-pole connection

a Conventional machine
b Transverse-flux machine

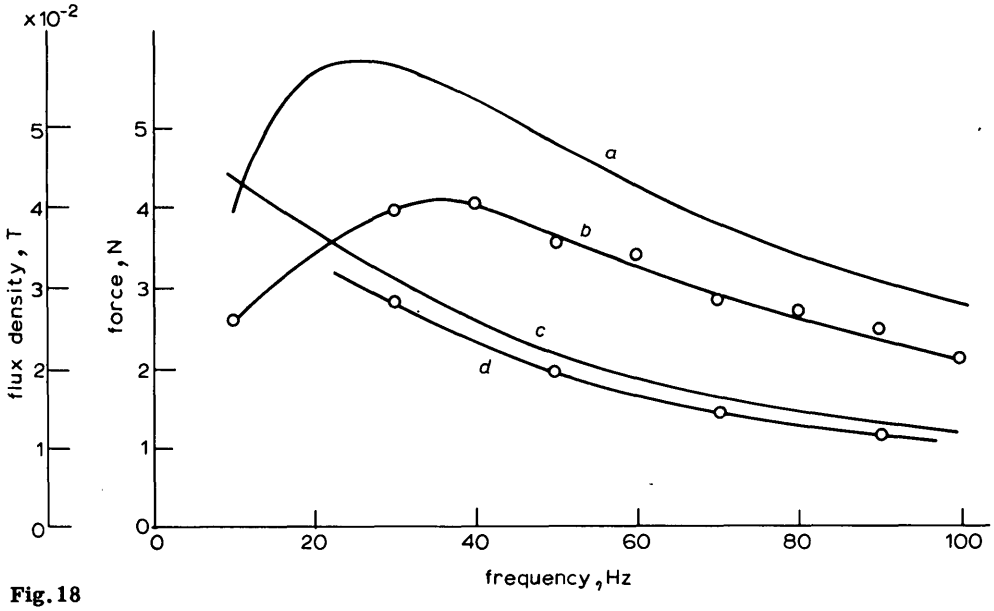

Fig. 18

Force and core-flux density at constant current for transverse-flux machine with 2-pole connection

a Theoretical force
b Measured force
c Theoretical flux density
d Measured flux density

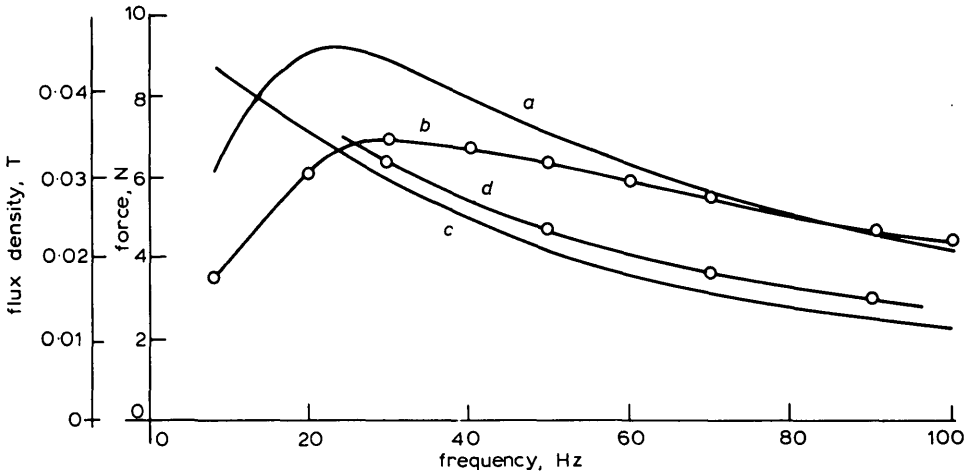

Fig. 19

Force and core-flux density at constant current for transverse-flux machine with 4-pole connection

a Theoretical force
b Measured force
c Theoretical flux density
d Measured flux density

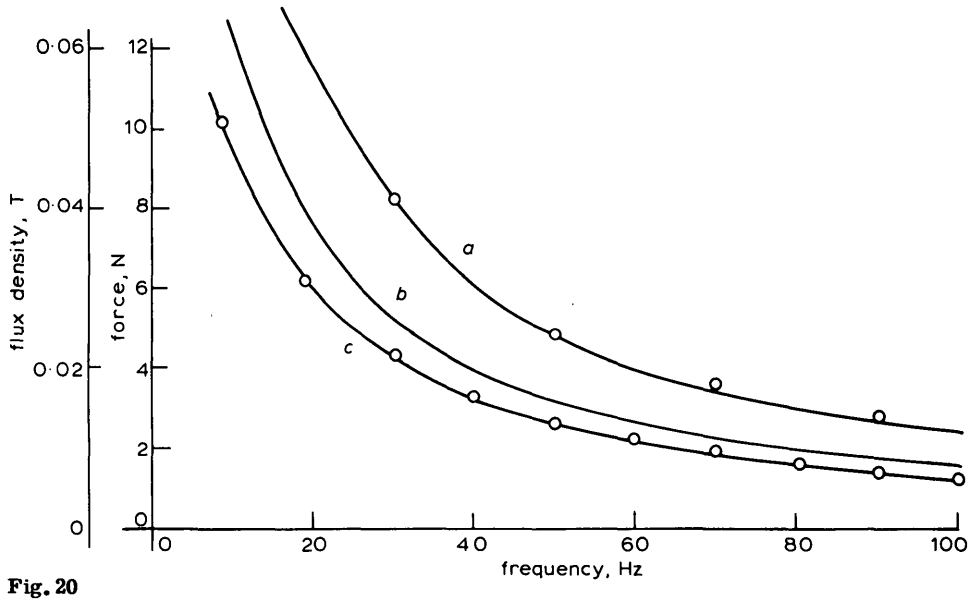

Fig. 20

Force and core-flux density at constant current for conventional machine with 2-pole connection

a Flux density
— theoretical results
○○○ measured results
b Theoretical force
c Measured force

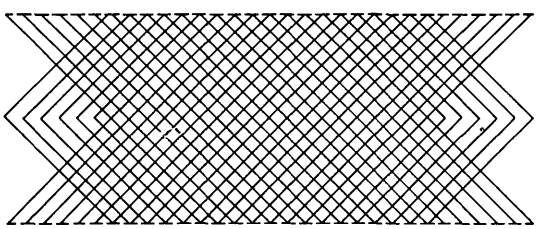

Fig. 21

Developed view of winding layers in transverse motor

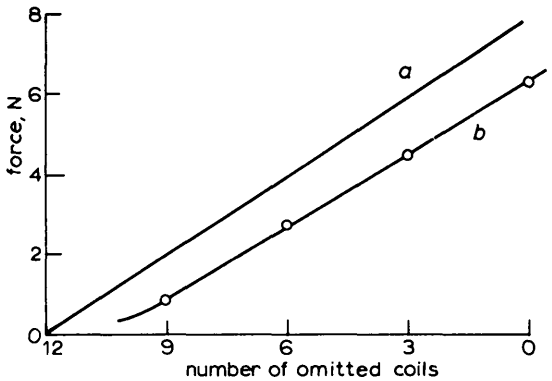

Fig. 22

Forces with omitted coils for transverse-flux 4-pole connection at 50 Hz

a Theoretical
b Measured

expected, since, as the excitation length is reduced, the sections of incomplete winding become relatively more important. The ratio of the measured and calculated forces for full-length excitation corresponds approximately to the ratio of the area covered by the complete excitation to $2(\pi/d_a)^2$. It was therefore felt that all the calculated results should be multiplied by this area ratio to allow for the ends. It must be emphasised that the confirmatory experimental results have been performed at only one frequency, and the factor must be applied with some caution.

5.3.4 Force measurements on the two models

The measured and predicted standstill forces at constant excitation currents for various arrangements are shown in Figs. 18-20.

To compare the performance of the two machines at a given core-flux density, the forces were scaled to a constant core-flux density using the previous results. The comparison between the forces in the 4-pole connections showed that the performances of the two machines were about equal; however, in the 2-pole connection, the transverse-flux motor produced about twice the force of the conventional motor, as shown in Fig. 23, which also shows the theoretical values.

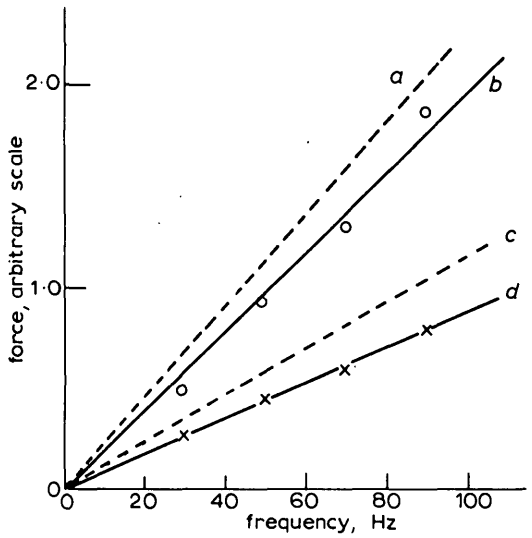

Fig. 23

Force at constant core-flux density for 2-pole connection

a Transverse, theroetical
b Transverse, measured
c Conventional, theoretical
d Conventional, measured

6 CONCLUSIONS

The new machines are useful when the core flux is the limiting design factor. In the comparisons attempted in this paper, only standstill forces have been considered. It will be appreciated that this is the most pessimistic comparison as far as the new machines are concerned; the core fluxes are, of course, at their lowest values at standstill for a particular current loading.

The analysis was performed on the assumption of sinusoidal conditions in the axial direction, i.e. for an infinite length. The predicted fluxes agreed more closely than the forces with the experimental results. This is thought to be due to the endwinding effects. It is possible that, if the true force per square metre could be measured locally at the middle of the tube, as could the flux, this would show a better agreement with theory.

7 ACKNOWLEDGMENTS

The authors are indebted to C. J. Carpenter, E. M. Freeman and H. R. Bolton for many useful discussions, and to Prof. E. R. Laithwaite for his support, guidance and encouragement. The authors are also grateful to C. Johnson, who constructed the experimental models.

8 REFERENCES

1 NIX, G. F., and LAITHWAITE, E. R.: 'Linear induction motors for low-speed and standstill application', Proc. IEE, 1966, **113**, (6), pp. 1044-1056
2 LAITHWAITE, E. R., EASTHAM, J. F., BOLTON, H. R., and FELLOWS, T. G.: 'Linear motors with transverse flux', ibid., 1971, **118**, (12), pp. 1761-1767
3 WELLS, A.: 'Library program to calculate Bessel functions of general complex argument'. King's College Computer Unit Program Library, 1969
4 PIPES, L. A.: 'Matrix theory of skin effect in laminations', J. Franklin Inst., 1956, **262**, pp. 127-138
5 GREIG, J., and FREEMAN, E. M.: 'Travelling-wave problem in electrical machines', Proc. IEE, 1967, **114**, (11), pp. 1681-1683
6 CULLEN, A. L., and BARTON, T. H.: 'A simplified electromagnetic theory of the induction motor, using the concept of wave impedance', ibid., 1959, **105C**, pp. 331-336
7 FREEMAN, E. M.: 'Travelling waves in induction machines: input impedance and equivalent circuits', ibid., 1968, **115**, (12), pp. 1772-1776
8 FREEMAN, E. M., and SMITH, B. E.: 'Surface-impedance method applied to multilayer cylindrical induction devices with circumferential exciting currents', ibid., 1970, **117**, (10), pp. 2012-2013
9 PRESTON, T. W., and REECE, A. B. J.: 'Transverse edge effects in linear induction motors', ibid., 1969, **116**, (6), pp. 973-979, and corrigenda, ibid., 1970, **117**, (9), p. 1808
10 FREEMAN, E. M., and LOWTHER, D. A.: 'Transverse edge effects in linear induction motors', ibid., 1971, **118**, (12), pp. 1820-1821

9 APPENDIX

Calculation of the transfer-matrix elements

From eqns. 21-24,

$$a_m = -r_m[Y_2\{K_n(\alpha_m r_{m-1})I_n(\alpha_m r_m) - I_n(\alpha_m r_{m-1})K_n(\alpha_m r_m)\} - \alpha_m\{K_n(\alpha_m r_m)I_{n-1}(\alpha_m r_{m-1}) + I_n(\alpha_m r_m)K_{n-1}(\alpha_m r_{m-1})\} \quad (43)$$

$$b_m = -j\omega\mu_m r_m\{I_n(\alpha_m r_m)K_n(\alpha_m r_{m-1}) - K_n(\alpha_m r_m)I_n(\alpha_m r_{m-1})\} \quad (44)$$

$$c_m = \frac{-jr_m}{\omega\mu_m}\Big[Y_1Y_2\{I_n(\alpha_m r_m)K_n(\alpha_m r_{m-1}) - K_n(\alpha_m r_m)I_n(\alpha_m r_{m-1})\} + Y_2\alpha_m\{I_{n-1}(\alpha_m r_m)K_n(\alpha_m r_{m-1}) + K_{n-1}(\alpha_m r_m)I_n(\alpha_m r_{m-1})\} - Y_1\alpha_m\{K_{n-1}(\alpha_m r_{m-1})I_n(\alpha_m r_m) + K_n(\alpha_m r_m)I_{n-1}(\alpha_m r_{m-1})\} + \alpha_m^2\{K_{n-1}(\alpha_m r_m)I_{n-1}(\alpha_m r_{m-1}) - K_{n-1}(\alpha_m r_{m-1})I_{n-1}(\alpha_m r_m)\}\Big] \quad (45)$$

$$d_m = r_m[Y_1\{I_n(\alpha_m r_m)K_n(\alpha_m r_{m-1}) - K_n(\alpha_m r_m)I_n(\alpha_m r_{m-1})\} + \alpha_m\{I_{n-1}(\alpha_m r_m)K_n(\alpha_m r_{m-1}) + K_{n-1}(\alpha_m r_m)I_n(\alpha_m r_{m-1})\}] \quad (46)$$

$$\text{where } Y_1 = \frac{2r_m k^2}{n^2 + r_m^2 k^2} - \frac{n}{r_m} \quad (47)$$

$$\text{and } Y_2 = \frac{2r_{m-1}k^2}{n^2 + r_{m-1}^2 k^2} - \frac{n}{r_{m-1}} \quad (48)$$